CHANGES IN HEAT INDEX ASSOCIATED WITH CO_2-INDUCED GLOBAL WARMING *

THOMAS L. DELWORTH, J. D. MAHLMAN and THOMAS R. KNUTSON
Geophysical Fluid Dynamics Laboratory/NOAA, Princeton, NJ 08542, U.S.A.

Abstract. Changes in Heat Index (a combined measure of temperature and humidity) associated with global warming are evaluated based on the output from four extended integrations of the GFDL coupled ocean-atmosphere climate model. The four integrations are: a control with constant levels of atmospheric carbon dioxide (CO_2), a second integration in which an estimate of the combined radiative forcing of greenhouse gases and sulfate aerosols over the period 1765–2065 is used to force the model, and a third (fourth) integration in which atmospheric CO_2 increases at the rate of 1% per year to double (quadruple) its initial value, and is held constant thereafter. While the spatial patterns of the changes in Heat Index are largely determined by the changes in surface air temperature, increases in atmospheric moisture can substantially amplify the changes in Heat Index over regions which are warm and humid in the Control integration. The regions most prone to this effect include humid regions of the Tropics and summer hemisphere extra-tropics, including the southeastern United States, India, southeast Asia and northern Australia.

1. Introduction

Projections from the latest generation of climate models (Kattenberg et al., 1995) suggest that global surface air temperature will increase substantially in the future due to the radiative effects of enhanced atmospheric concentrations of greenhouse gases. A number of studies have explored the potential changes in the climate system associated with global warming (Kattenberg et al., 1995; Warrick et al., 1995; Santer et al., 1995, and references therein). Other studies have explored the impact of global climate change on the spread of disease (Stone, 1995).

In this study we examine a very direct measure of the impact of global warming on human health and comfort. The Heat Index (defined in the next section) is a measure of the combined effects of temperature and atmospheric moisture on the ability of the human body to dissipate heat. Periods of very high Heat Index have been associated with adverse human health consequences (Kalkstein et al., 1993), and there is some observational evidence of upward trends in summer Heat Index values over the United States in recent decades (Gaffen and Ross, 1998). It is the intent of this paper to examine the changes in Heat Index simulated by a coupled ocean-atmosphere climate model in response to altered radiative forcing. These

Climatic Change **43:** 369–386, 1999.

results illustrate the important extra burden that enhanced levels of atmospheric water vapor may place on human comfort as a consequence of global warming.

2. Definition of Heat Index

Steadman (1979, 1984, 1994) developed the 'Heat Index' (also called 'apparent temperature') as a means to quantify the effects of various environmental factors, including wind, radiation, and atmospheric moisture content, on the ability of the human body to dissipate heat. The Heat Index (as used in this study, and which we refer to as the 'Steadman Heat Index') is a measure of the stress imposed on humans by elevated levels of atmospheric moisture (this version of the index neglects the effects of wind and radiation changes). These conditions inhibit the ability of the body to dissipate heat through evaporation, thereby causing discomfort. Specifically, for a given atmospheric temperature and water vapor pressure, the Steadman Heat Index (SHI) is defined as the temperature that would produce an equivalent stress on the body if the water vapor pressure were changed to a predetermined reference pressure (specifically, 1.6 kPa, which is the saturation vapor pressure of water at 14 °C). For example, an air temperature of 30 °C with a relative humidity of 60 percent translates to an apparent temperature (heat index) of 33 °C. The difference between the SHI and air temperature is a measure of the heat stress placed on the human body by elevated atmospheric water vapor content. Note that the SHI can be less than the air temperature when the atmospheric vapor pressure is less than the reference amount, indicating the enhanced ability of the body to dissipate heat through evaporation under dry conditions (such as typically found in desert and mountainous regions).

The relationship between temperature, humidity, and the SHI is illustrated in Figure 1, which shows the SHI as a function of temperature for two different (constant) levels of relative humidity. These curves are meant to depict the functional form of the SHI, and are not a projection of any future conditions. Note that the relationship is nonlinear, and that the slope increases with temperature. Further, the slope and curvature are larger (at a given temperature) for the case with higher relative humidity. Both of these features are a consequence of the approximately exponential dependence on temperature of the saturation vapor pressure of water vapor (as described by the Clausius–Clapeyron equation, also displayed in Figure 1). Note that values of SHI are not plotted for values of temperature and relative humidity which exceed the range over which the calculation of the SHI is valid.

An inspection of the curves in Figure 1 shows that for a specified increase of temperature, with constant relative humidity, the increase in SHI will be larger for (i) higher initial temperatures, and (ii) larger relative humidity values. Note also that the difference between air temperature and the SHI increases as a function of temperature (this is illustrated by the increasing distance between the solid curves and the darker dashed line as temperature increases). Therefore, as the temperature

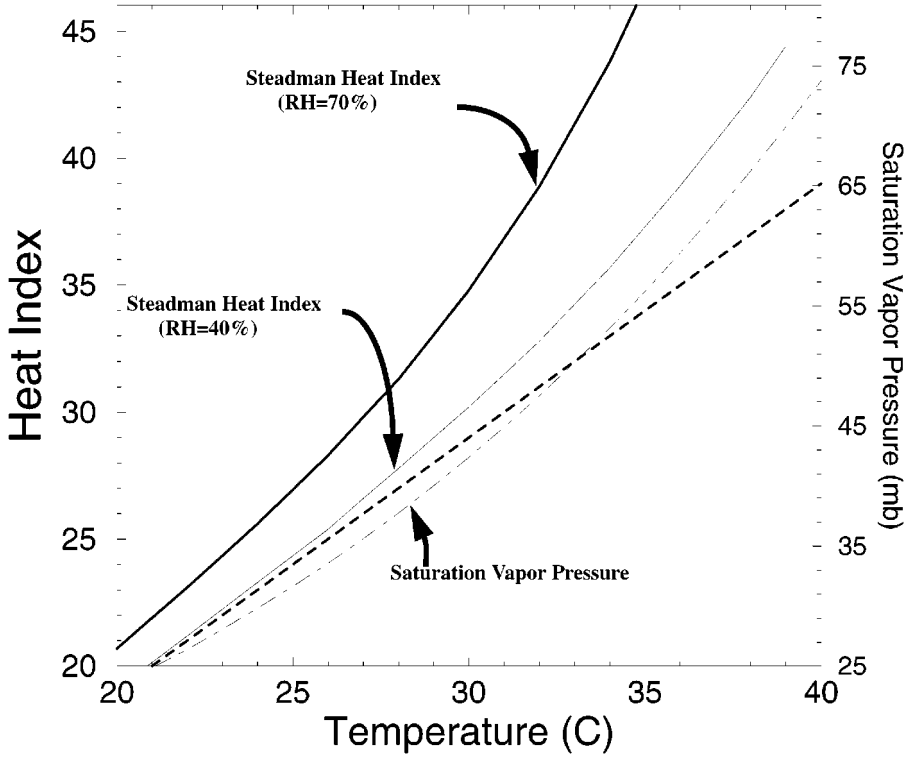

Figure 1. Dependence of Steadman Heat Index on air temperature and relative humidity. The two solid lines denote Heat Index as a function of temperature for two cases with differing levels of (constant) relative humidity. The dashed line is used as a reference with slope of 1. The differences between either solid line and the dashed line denotes the difference between the Steadman Heat Index and the temperature (this difference is referred to later in the text as the 'moisture-induced stress'). For reference, the dot-dashed line shows the dependence of saturation vapor pressure (right ordinate) on temperature.

increases under enhanced levels of greenhouse gases, the difference between the SHI and the air temperature (a measure of the stress on the body due to enhanced moisture levels, which we shall refer to as the 'moisture-induced stress') will increase as the moisture content of the atmosphere increases (unless a pronounced decrease in relative humidity occurs, which model projections indicate is unlikely – this is examined below). The moisture-induced stress can be appreciable, even for unchanged relative humidity. As illustrated by these curves, such an effect is expected to be most pronounced in regions which are already both warm and humid. It is this increase which is the subject of this paper.

Steadman (1979, 1984, 1994) describes extensive and detailed efforts to quantify the impact on human comfort of elevated levels of atmospheric moisture. While different methodologies may result in different quantitative measures, the underlying physical principles are robust. As the atmosphere is warmed its ability

to hold moisture increases approximately exponentially. With the exception of a dramatic decrease in relative humidity as the air warms, the absolute moisture content of the air will increase. Since evaporative cooling of the body is inhibited by atmospheric moisture content, elevated levels of atmospheric moisture will generally cause increased human discomfort. While the quantification of this effect has uncertainties, the underlying physical principles are the laws of moist-air thermodynamics. In fact, the remaining uncertainties in the model-based projections of future warming are very likely to be greater than the uncertainties associated with the details of the Heat Index calculation.

3. Description of Model Integrations Used

The changes in the SHI associated with global warming are evaluated based on the output of three multi-century integrations of the GFDL coupled ocean-atmosphere climate model subject to time-varying concentrations of greenhouse gases and (in one case) aerosols, along with a control integration. The coupled model consists of separate atmospheric and oceanic components which interact through the exchange of heat, fresh water, and momentum at the air-sea interface (for details of the model formulation and experimental designs see Manabe and Stouffer (1994) and references therein). The model is forced with a seasonal cycle of insolation at the top of the atmosphere, but there is no diurnal cycle. The model is global in extent, with geography consistent with its resolution.

The atmospheric component has an approximate resolution of 7.5° longitude by 4.5° latitude, with 9 unevenly spaced layers in the vertical. Energy and water balances are computed over land surfaces. The ocean component has an approximate resolution of 3.7° in longitude and 4.5° in latitude, with 12 unevenly spaced layers in the vertical. A simple sea-ice model is used. Adjustments of the heat and fresh water fluxes, determined from preliminary integrations of the separate model components, are applied at the air-sea interface to help keep the model's climate near a realistic mean state. These adjustments do not vary from one year to the next.

The first integration, a control experiment with an atmospheric CO_2 concentration of 300 ppm, is 1000 years in length. In the second experiment an estimate of the combined radiative forcing of greenhouse gases and the direct effect of sulfate aerosols over the period 1765–2065 is used to force the model (Haywood et al., 1997). This 300 year integration (hereafter referred to as the 'transient aerosol' experiment) started from an arbitrary point in the control integration. Haywood et al. (1997) demonstrated that while increasing greenhouse gases tend to warm the model's climate, enhanced levels of atmospheric sulfate aerosols can potentially offset this warming. However, the relative cooling by sulfate aerosols diminishes as the greenhouse gas concentration increases. In the third (fourth) experiment, atmospheric CO_2 levels increase at the rate of 1% per year until the CO_2 concen-

tration is double (quadruple) the initial value; thereafter, the CO_2 concentration is held constant. The third (fourth) experiment will be referred to hereafter as the '$2 \times CO_2$' ('$4 \times CO_2$') case. The third and fourth experiments were 500 years in length.

4. Simulated Changes for the Transient Aerosol Experiment

We first examine simulated changes in the transient aerosol experiment. This experiment is designed to estimate the response of the Earth's climate system to a representation of radiative forcing changes from greenhouse gas and sulfate aerosol changes over the period 1765–2065. In Section 5 we will examine changes for additional experiments using more idealized time series of radiative forcing (the $2 \times CO_2$ and $4 \times CO_2$ experiments).

4.1. ATMOSPHERIC MOISTURE

Since the SHI is affected by atmospheric moisture as well as temperature, it is desirable to evaluate the changes of near-surface atmospheric moisture content associated with the transient aerosol experiment. Long-term means were computed for July using all 1000 years of the control experiment and years 2011–2040 of the transient aerosol experiment (see Haywood et al., 1997, for a depiction of the changes with time of global mean surface air temperature for this experiment). The period 2011–2040 was chosen for study as an indicator of potential climate changes over the next several decades; this averaging period is used for all results shown from the transient aerosol experiment. Shown in Figure 2 are the changes in specific and relative humidity for July between the two experiments. Figure 2a indicates that near-surface atmospheric specific humidity increases at almost all locations on the globe. The increases are largest over the tropics and middle latitudes of the summer hemisphere. There is also an increase in oceanic evaporation (not shown) associated with the global scale increase of surface air temperature (shown below).

In contrast, Figure 2b shows that changes in relative humidity are near zero over most oceanic regions, with some decreases of up to 8% over the continental interiors of North America, Europe and Asia. These continental decreases are related to significant changes in the land-surface hydrologic balance (Wetherald and Manabe, 1995) associated with global warming. In spite of the decrease in relative humidity, specific humidity still increases over those continental locations, thus denoting greater total water vapor in the near-surface atmosphere. The increases in total water vapor contribute to the increases in SHI shown below.

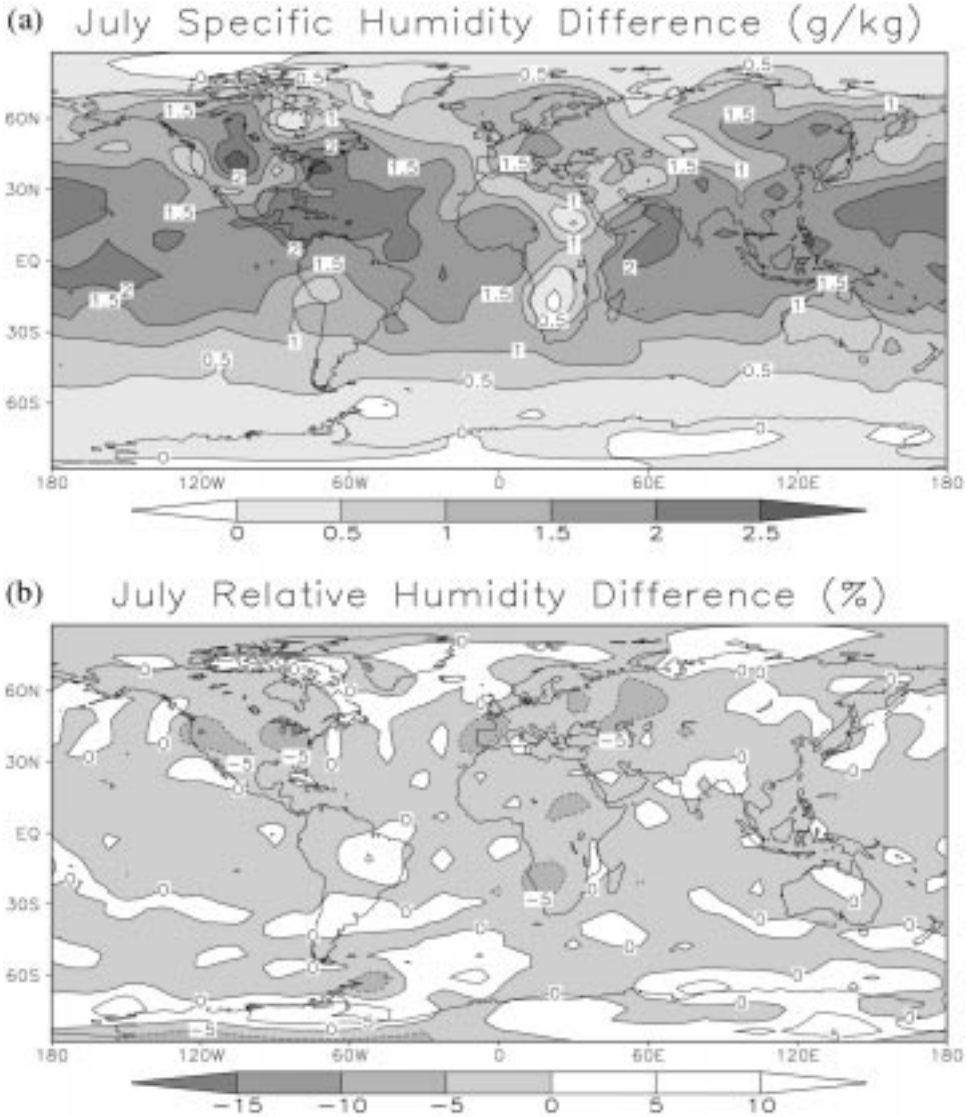

Figure 2. Differences for July between the transient aerosol experiment (years 2011–2040) and the long-term mean of the control integration for (a) near-surface specific humidity (g/kg) and (b) near-surface relative humidity. The relative humidity difference is computed as the percentage saturation in the transient aerosol experiment minus the percentage saturation in the control experiment.

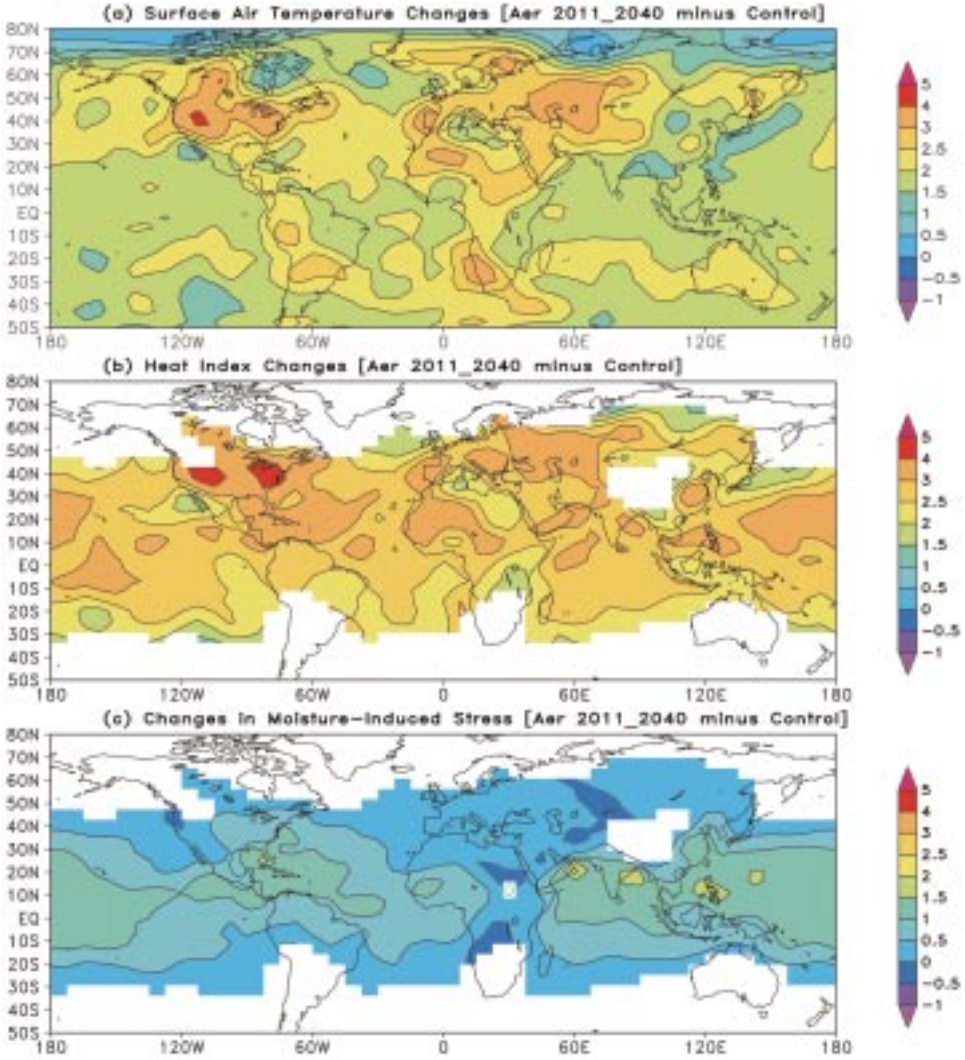

Figure 3. (a) Time-mean differences of near-surface air temperature (in °C) between the transient aerosol integration and the Control integration (see text for experiment details). The time-means were computed for July using years 1–1000 of the Control integration and years 2011–2040 of the transient aerosol integration. (b) Same as (a) except using Heat Index. Heat Index values are not defined for temperatures less than 10 °C; such regions are left blank (primarily mountainous and high latitude locations). (c) Time-mean difference between 'moisture-induced stress' in transient aerosol experiment and 'moisture-induced stress' in Control (the term 'moisture-induced stress' is defined in text).

4.2. CHANGES IN NEAR-SURFACE AIR TEMPERATURE AND SHI

The other term contributing to changes in SHI is near-surface air temperature. Shown in Figure 3a is a spatial map of the changes in near-surface air temperature between the transient aerosol and control experiments. Temperature changes are largest in the Northern (summer) Hemisphere mid-latitude continental regions, although there are substantial changes in the Tropics and Southern Hemisphere sub-tropics. The warming over the oceans results in increased evaporation.

Monthly mean near-surface air temperature and relative humidity values were used to compute the SHI from linear interpolation of the values in a table from Steadman (1996, personal communication; this is a slightly updated version of Table 3 in Steadman, 1994). Shown in Figure 3b are the differences of the SHI for July between the transient aerosol and control experiments. The spatial pattern of the SHI differences is generally similar to that of the temperature changes, indicating that temperature changes are the dominant term in creating changes in the SHI. The magnitude of the SHI increase is generally larger than the temperature increases, denoting the substantial additive role that atmospheric moisture plays. One measure of that role is indicated by the difference between the SHI and surface air temperature, referred to above as the 'moisture-induced stress'. Where this term is positive (i.e., SHI values greater than the surface air temperature) atmospheric moisture is adding to the heat stress on the body. The differences in the moisture-induced stress between the transient aerosol experiment and the control were evaluated for July, and are displayed in Figure 3c. Note that this quantity can be expressed as:

$$\text{difference in 'moisture-induced stress'} = [\text{SHI} - \text{SAT}]_{\text{aerosol}} - [\text{SHI} - \text{SAT}]_{\text{control}},$$

where 'SAT' is surface air temperature (lowest model atmospheric level). Positive values of this difference indicate that atmospheric moisture changes are amplifying the changes in the SHI (i.e., the SHI exceeds the surface air temperature by a larger margin in the transient aerosol integration than in the Control integration). As one might surmise from the discussion in Section 2, the differences are largest in tropical and subtropical regions which were already warm and moist. The differences approach or exceed 1 °C in the southeastern United States, the Caribbean, the northern Indian Ocean and adjoining continental regions, parts of southeast Asia, and the western tropical Pacific. These moisture effects account for up to 35% of the increases in the SHI. Note the substantial increases in specific humidity in these regions (see Figure 2a). It must be pointed out, however, that this model has a bias towards excessive relative humidity over oceanic regions in the control integration. In contrast, there is only a small difference in moisture-induced stress over the arid regions of northern Africa, the Middle East, central Asia and south central Africa, where the increases in specific humidity are relatively small.

While July near-surface air temperature increases are largest over the midlatitude continental interiors, the differences in 'moisture-induced stress' are more

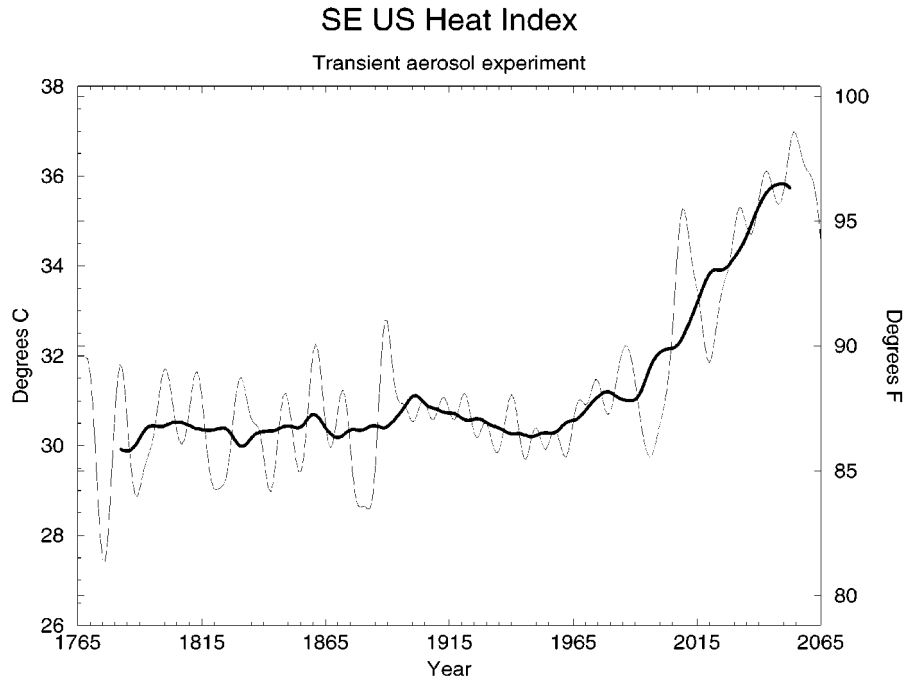

Figure 4. Time series of SHI averaged over the southeastern United States (94° W–79° W, 31° N–40° N) for the transient aerosol experiments. Only values from July are plotted. The heavy (thin) line shows the time series after applying a 40 (10) year low-pass filter.

closely linked to coastal and oceanic regions (see Figure 3c). One of the principal reasons for this is that summer soil moisture decreases substantially in mid-latitude interiors in the transient aerosol experiment (as well as the $2 \times CO_2$ and $4 \times CO_2$ experiments to be discussed later). This phenomenon is referred to as 'summer drying' (see Wetherald and Manabe, 1995, for further discussion). The soil moisture decreases are associated with reductions in relative humidity during July of up to 8% over central North America in the transient aerosol integration compared to the Control integration (see Figure 2b). This feature tempers the ability of atmospheric moisture to amplify the Heat Index increases in the continental interiors, resulting in a relatively larger moisture-induced stress over the more humid regions. The net effect is that the drier, midlatitude continental interiors experience larger temperature increases but the amplification of the Heat Index increases by moisture is relatively small. The more humid tropical and subtropical regions have smaller temperature increases but larger amplification of the Heat Index increases via the moisture effect.

The time series of July Heat Index values from the transient aerosol experiment averaged over a portion of the southeastern United States (94° W–79° W, 31° N–40° N) is shown in Figure 4. The ability of climate models to make projections on regional scales is limited, and thus this time series should not be interpreted as a

literal statement of expected conditions in the southeastern United States. Rather, this is an illustration of the temporal changes in the SHI in a region in which SHI increases are amplified by moisture increases due to the warm, humid nature of the climate in the Control integration (this amplification is shown in Figure 3c). The period 1765 to approximately 1995 has little trend in SHI. However, there are rapid increases in the SHI after the year 2000, consistent with the model-predicted increasing surface air temperature (see Haywood et al., 1997). Note that there are large swings in the SHI on time scales of several years to a decade or more. These are a manifestation of the internal variability of the system, and increase the difficulty of detecting climate change.

While the southeastern United States time series shown in Figure 4 should not be viewed as a forecast of regional climate change, it is still useful to assess the credibility of the model over this region. This was evaluated by gathering observed time series of air temperature and relative humidity from surface stations in this region, and using these to compute observed SHI values. The simulated means of surface air temperature and SHI for July in the control experiment were in fair agreement with the long term means of the observed temperature and SHI values for this region. The comparison also indicates, however, that this model has an apparent bias of substantially overestimating the temporal variability of both surface air temperature and SHI in this region during summer, related to excessive drying of the soil.

5. Simulated Changes for the 2 $\times$ CO_2 and 4 $\times$ CO_2 Experiments

The transient aerosol experiment provides a perspective on potential changes in atmospheric temperature, moisture, and SHI over the next several decades assuming a particular scenario of radiative forcing. It is also useful to examine changes that might occur on somewhat longer time scales assuming effective greenhouse gas concentrations in the atmosphere reach double or quadruple the pre-industrial levels.

Time-means were computed for the 30 years immediately after the CO_2 levels had reached double (quadruple) their initial values in the $2 \times CO_2$ ($4 \times CO_2$) experiments (these correspond to model years 71–100 and 141–170 for the $2 \times CO_2$ and $4 \times CO_2$ experiments respectively). It should be noted that for those time periods in the CO_2 experiments the model integrations had not yet achieved a thermal equilibrium with the new radiative forcings (which can take centuries to millennia).

Shown in Figure 5 are the changes in near-surface atmospheric specific and relative humidity for the $2 \times CO_2$ experiment. The patterns of these changes are similar to those from the transient aerosol experiment, but are somewhat larger in magnitude. In particular the magnitude of the reduction in relative humidity in the $2 \times CO_2$ integration over North America and Europe has increased to more

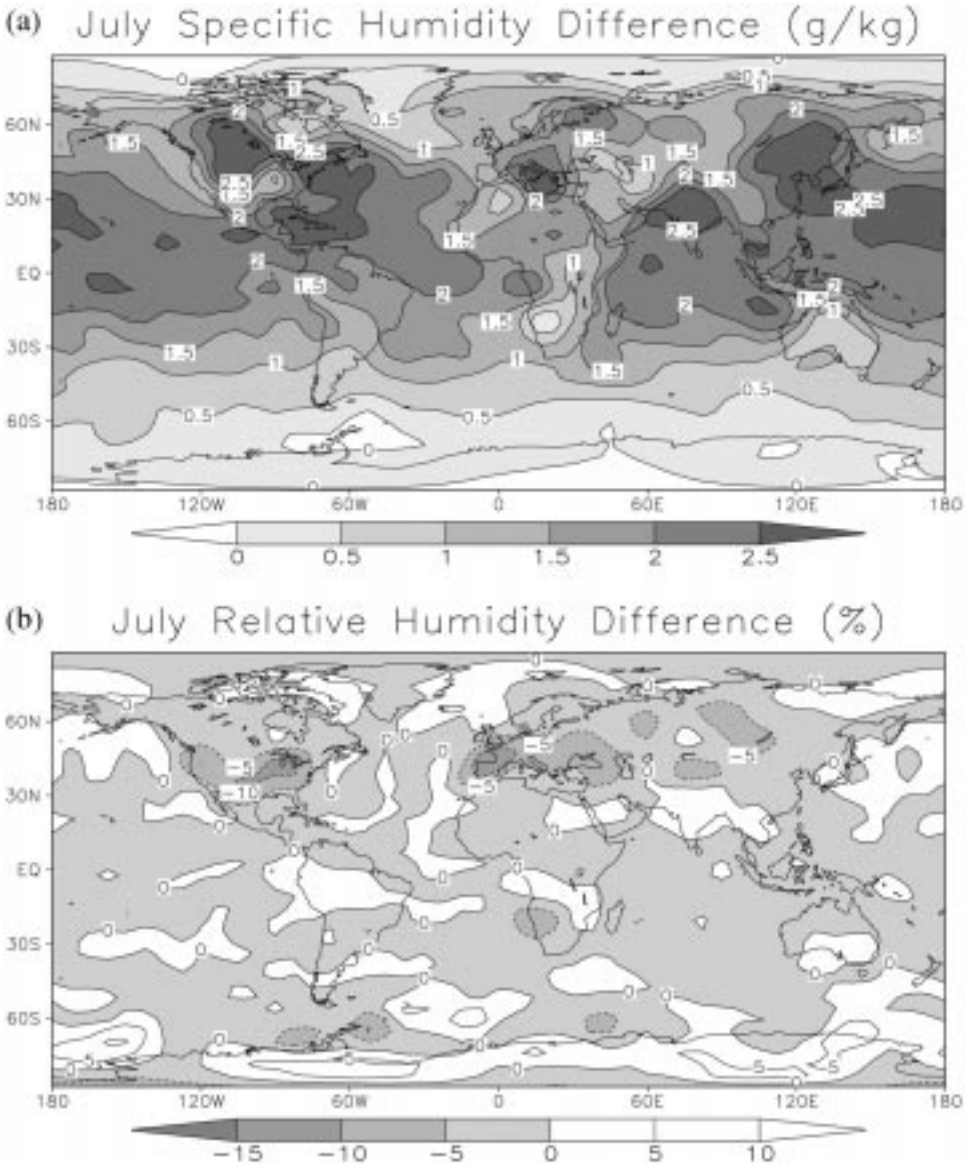

Figure 5. Differences for July between the $2 \times CO_2$ experiment (years 71–100) and the long-term mean of the control integration for (a) near-surface specific humidity (g/kg) and (b) near-surface relative humidity. The relative humidity difference is computed as the percentage saturation in the $2 \times CO_2$ experiment minus the percentage saturation in the control experiment.

than 10% in some areas. However, there is still a substantial increase in specific humidity over those regions.

The changes in near-surface air temperature, SHI, and 'moisture-induced stress' are shown in Figure 6 for the $2 \times CO_2$ experiment minus the control. The spatial patterns are quite similar to those from the transient aerosol experiment (see Figure 3), although somewhat larger in magnitude.

A more dramatic example of such changes is indicated in Figure 7, which shows changes of near-surface air temperature, SHI, and 'moisture-induced stress' between the $4 \times CO_2$ and the control experiments. The structure is similar to that for the transient aerosol and $2 \times CO_2$ experiments, but the magnitudes of the changes in surface air temperature, SHI, and moisture-induced stress are substantially larger.

The time series of July surface air temperatures and Heat Index values from the control, $2 \times CO_2$ and $4 \times CO_2$ experiments averaged over a portion of the southeastern United States (94° W–79° W, 31° N–40° N) are shown in Figure 8. Note that the changes in SHI are substantially larger than those of surface air temperature, thereby quantifying the effects of moisture. The larger increase of SHI relative to surface air temperature indicates the amplification of the SHI by atmospheric moisture.

The above suite of analyses (shown in Figures 2–8) were for the month of July. Similar analyses were performed for all calendar months. The effect of moisture changes on the increases of SHI varies with the seasonal cycle, and is largest in regions and seasons with warm, humid conditions. For example, in January (Figure 9) the largest differences in 'moisture-induced stress' in the $2 \times CO_2$ experiment occur in the Caribbean, parts of tropical and subtropical South America, southern Africa, the tropical Indian Ocean, northern Australia, and the western tropical Pacific and maritime continent. The results for the transient aerosol and $4 \times CO_2$ experiments (not shown) have a similar spatial pattern but differ in magnitude.

One limitation of the present study is that only monthly mean model output were available for analysis. In addition, a diurnal cycle of insolation was not incorporated in the model. Calculating the SHI using hourly data from a model with a diurnal cycle would likely lead to higher values of the SHI due to the non-linearity of the SHI. Further, as a result of both the higher variance of daily data and the non-linearity of the SHI, it is anticipated that individual days (and stretches of days) would have SHI increases considerably larger than the results presented for monthly means.

6. Summary and Conclusions

The Heat Index (also called apparent temperature) is a measure of the stress placed on humans by elevated levels of atmospheric temperature and moisture. As the atmospheric moisture content increases, the ability of the human body to release heat through evaporation is inhibited, thereby causing discomfort and stress.

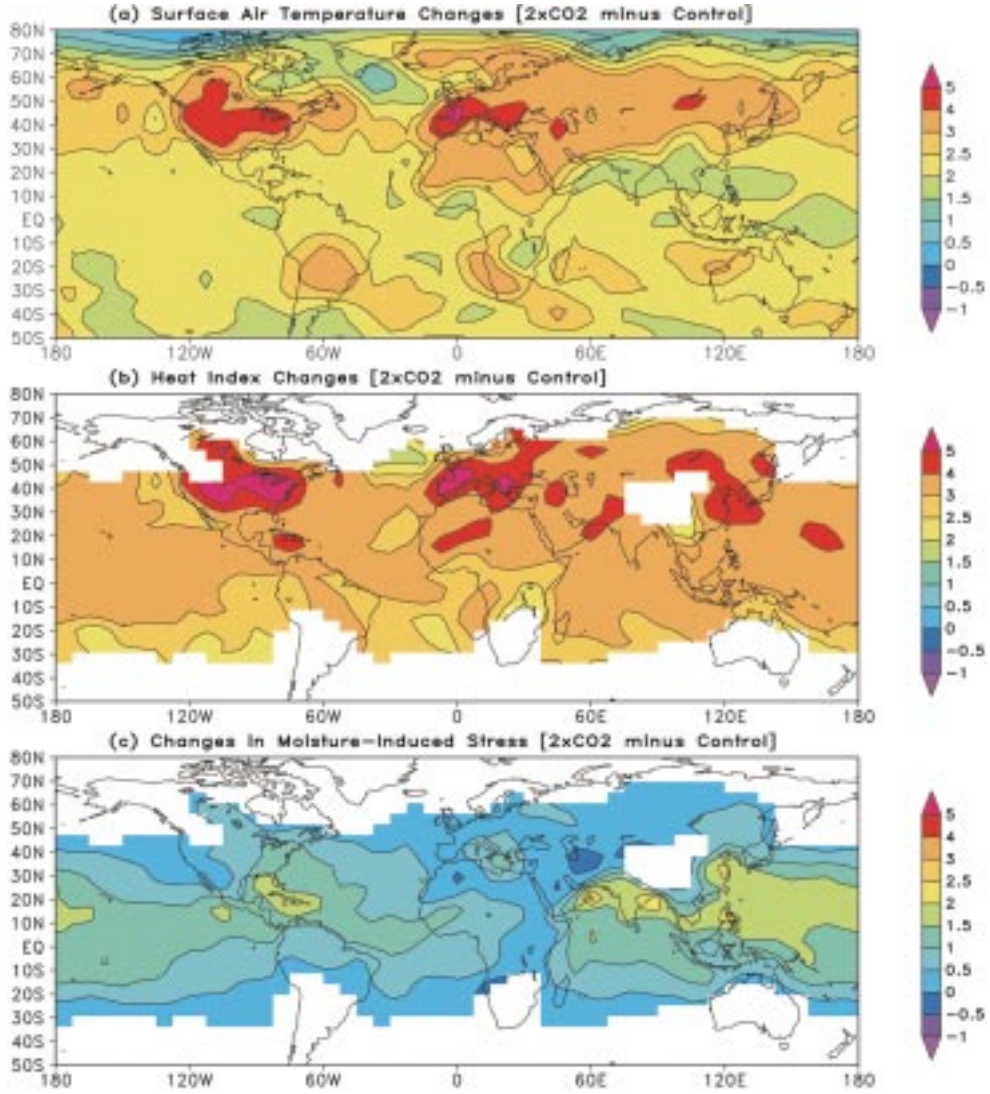

Figure 6. (a) Time-mean differences of near-surface air temperature (in °C) between experiment $2 \times CO_2$ and the Control integration (see text for experiment details). The time-means were computed for July using years 1–1000 of the Control integration and years 71–100 of the $2 \times CO_2$ integration. (b) Same as (a) except using Heat Index. Heat Index values are not defined for temperatures less than 10 °C; such regions are left blank (primarily mountainous and high latitude locations). (c) Time-mean difference between 'moisture-induced stress' in $2 \times CO_2$ experiment and 'moisture-induced stress' in Control (the term 'moisture-induced stress' is defined in text).

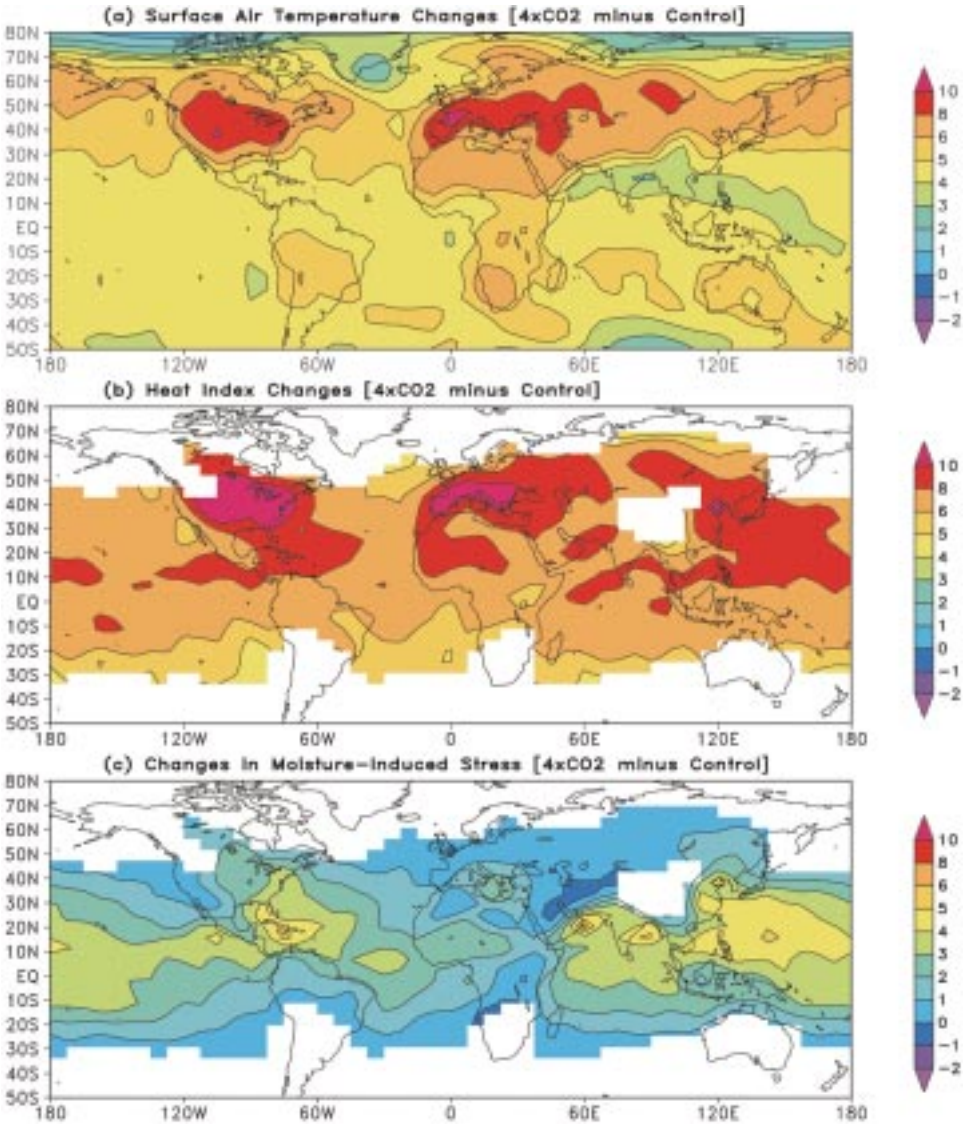

Figure 7. Same as Figure 6 except using differences between experiment 4 × CO_2 (years 141–170) and the Control. Note the change in the color shading levels versus Figure 6.

Changes in Heat Index associated with three different scenarios of global warming have been presented. In the first integration an estimate of the combined radiative forcing of greenhouse gases and the direct effect of sulfate aerosols over the period 1765–2065 is used to force the model. In the second (third) integration, atmospheric CO_2 increases at a rate of 1% per year to twice (four times) its initial value, and is held constant thereafter. It has been shown that changes in the Heat Index resulting from increases in atmospheric moisture can account for a consider-

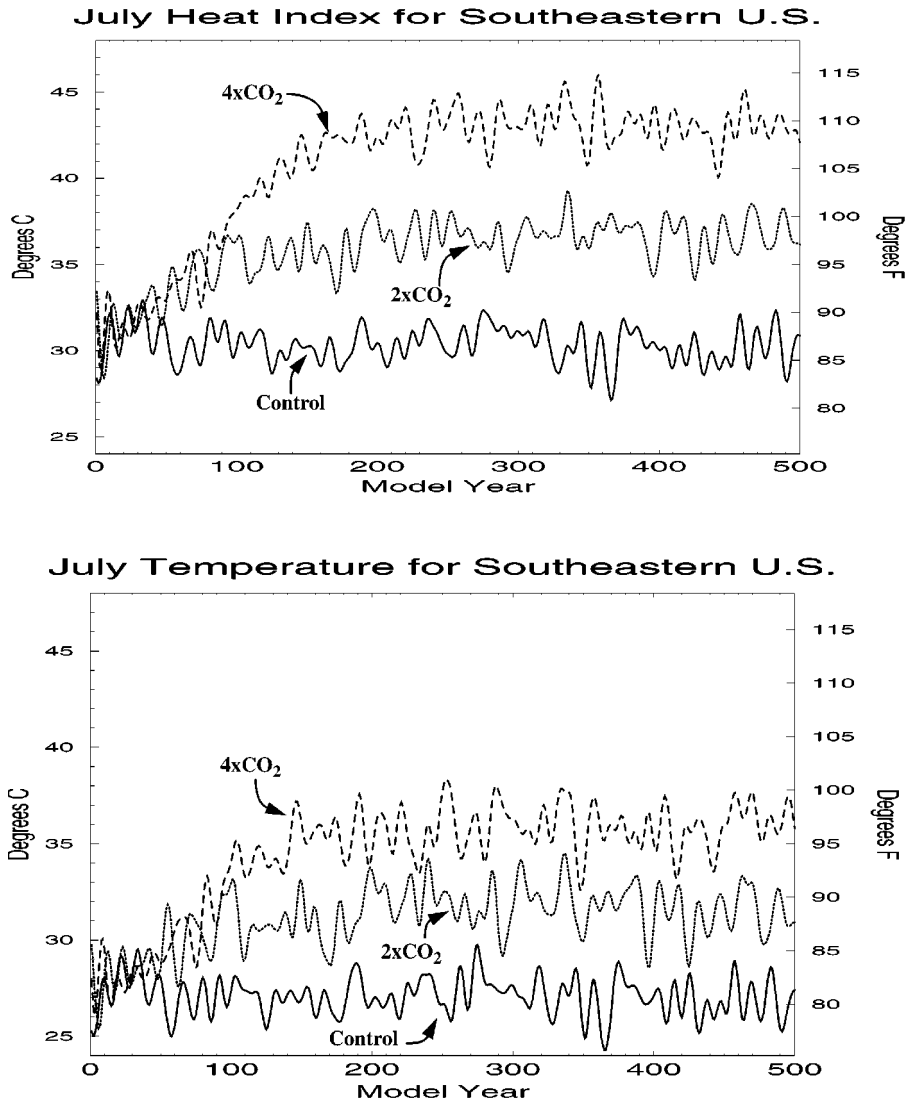

Figure 8. (a) Time series of surface temperature averaged over the southeastern United States for the three experiments. Only values from July are plotted. Prior to plotting, a 10 year low pass filter was applied to the time series. (b) Same as (a) for Heat Index. In the $4 \times CO_2$ experiment the combination of temperature and humidity is occasionally so large that Heat Index values are not defined (see text for discussion). In such cases, the spatial mean is computed using only those spatial locations with defined Heat Index values.

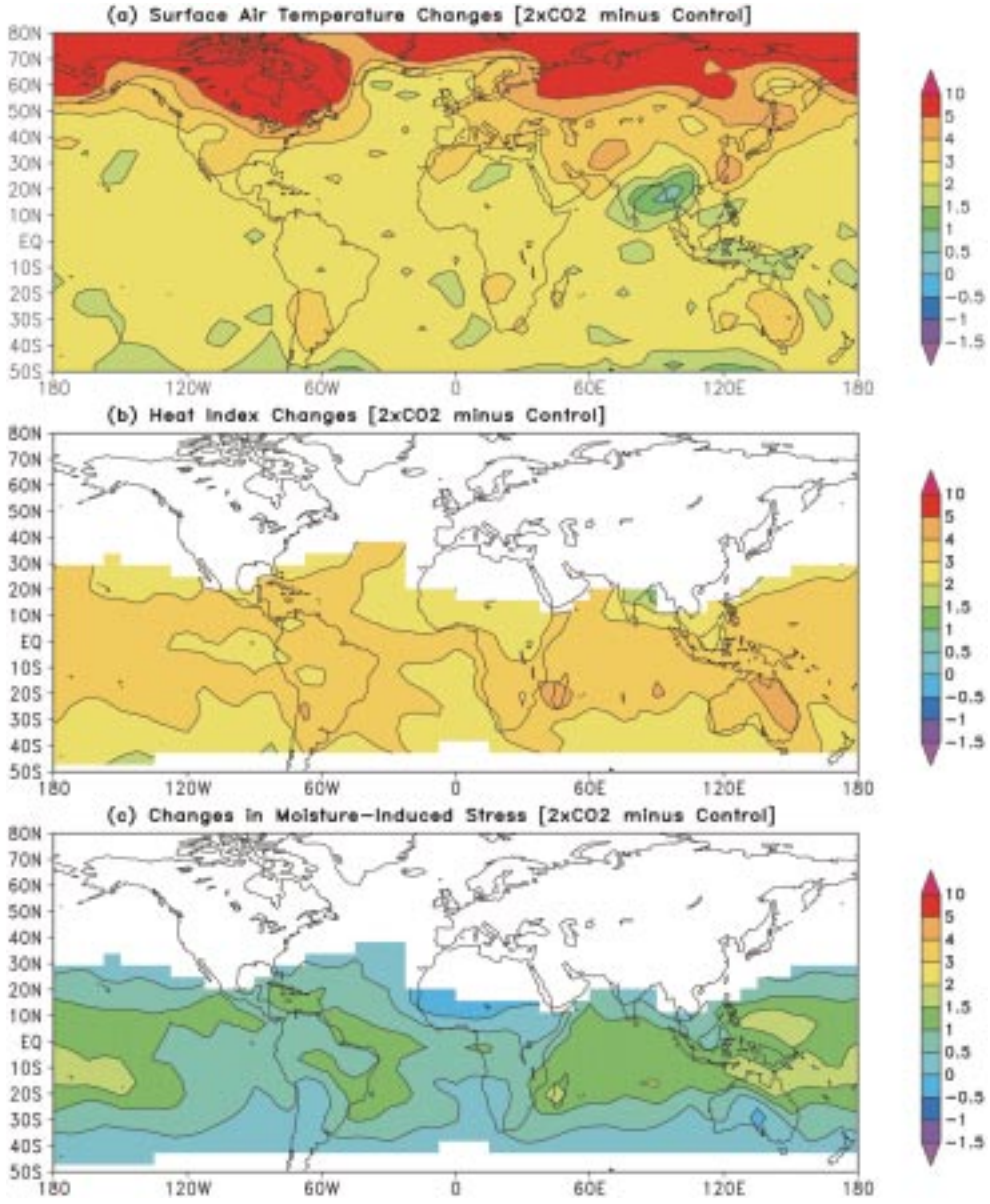

Figure 9. Same as Figure 6, using data from January.

able fraction (up to 35%) of the total increases in the Heat Index. These increases are largest over humid regions of the Tropics and summer hemisphere extra-tropics. Thus, in evaluating the potential impact of future climate change on human health and comfort, it must be stressed that changes in surface air temperature are only one part of the story. Changes in atmospheric moisture content also play a significant role, with potentially undesirable consequences.

It should be noted that the results presented here are from one particular numerical model. When subjected to a doubling of effective CO_2 concentrations the equilibrium response of the atmospheric model used in this study coupled to a mixed layer model of the ocean is 3.7 °C. This is in the upper half of the range of sensitivities (1.5 °C–4.5 °C) published in the 1995 IPCC report (see Kattenberg et al. 1995). In addition, regional features, such as summertime continental surface air temperatures, must be regarded as more uncertain than global mean temperatures. Similar calculations using data from other models could well produce results which are quantitatively different, but which we suspect would be qualitatively similar. Even a model with a significantly smaller sensitivity to greenhouse gas increases would still exhibit this effect, albeit with reduced amplitude. The fundamental physical relationships governing these results are the laws of thermodynamics. As the atmosphere warms its ability to hold moisture increases; this translates into an increased stress on the human body, the magnitude of which is dictated by the magnitude of the temperature and moisture increases.

Acknowledgements

The authors would like to express their thanks to Ron Stouffer and Syukuro Manabe for use of the output from several numerical experiments, and to Anthony Broccoli, Dian Gaffen, Isaac Held, John Lanzante, Chris Milly, Robert Steadman, Ron Stouffer, and two anonymous reviewers for useful comments on a preliminary version of this manuscript.

References

Gaffen, D. J. and Ross, R. J.: 1998, 'Increased Summertime Heat Stress in the U.S.', *Nature* **396**, 529–530.

Haywood, J. M., Stouffer, R. J., Wetherald, R. T., Manabe, S., and Ramaswamy, V: 1997, 'Transient Response of a Coupled Model to Estimated Changes in Greenhouse Gas and Sulfate Concentrations', *Geophys. Res. Lett.* **24**, 1335–1338.

Kalkstein, L. S. and Smoyer, K. E.: 1993, 'The Impact of Climate Change on Human Health: Some International Implications', *Experientia* **49**, 969–979.

Kattenberg, A., Giorgi, F., Grassl, H., Meehl, G. A., Mitchell, J. F. B., Stouffer, R. J., Tokioka, T., Weaver, A. J., and Wigley, T. M. L.: 1995, 'Climate Models – Projections of Future Climate', in *Climate Change 1995 – The Science of Climate Change*, Chapter 6, Cambridge University Press.

Manabe, S. and Stouffer, R. J.: 1994, 'Multiple-Century Response of a Coupled Ocean-Atmosphere Model to an Increase of Atmospheric Carbon Dioxide', *J. Climate* **7**, 5–23.

Santer, B. D., Wigley, T. M. L., Barnett, T. P., and Anyamba, E.: 1995, 'Detection of Climate Change and Attribution of Causes', in *Climate Change 1995 – The Science of Climate Change*, Chapter 8, Cambridge University Press.

Steadman, R. G.: 1979, 'The Assessment of Sultriness. Part I: A Temperature-Humidity Index Based on Human Physiology and Clothing Science', *J. Appl. Meteorol.* **18**, 861–873.

Steadman, R. G.: 1984, 'A Universal Scale of Apparent Temperature', *J. Clim. Appl. Meteorol.* **23**, 1674–1687.
Steadman, R. G.: 1994, 'Norms of Apparent Temperature in Australia', *Aust. Met. Mag.* **43**, 1–16.
Stone, R.: 1995, 'If the Mercury Soars, So May Health Hazards', *Sci. News Comments* **267**, 957–958.
Warrick, R. A., Le Provost, C., Meier, M. F., Oerlemans, J., and Woodworth, P. L.: 1995, 'Changes in Sea Level', in *Climate Change 1995 – The Science of Climate Change*, Chapter 7, Cambridge University Press.
Wetherald, R. and Manabe, S.: 1995, 'The Mechanisms of Summer Drying Induced by Greenhouse Warming', *J. Climate* **8**, 3096–3108.

(Received 13 February 1998; in revised form 1 December 1998)